



Tectonic patterns of shortening landforms in Mercury's northern smooth plains

Kelsey T. Crane*, Christian Klimczak

Structural Geology and Geomechanics Group, Department of Geology, University of Georgia, Athens, GA 30602, USA

ARTICLE INFO

Keywords:
 Thrust faulting
 Tectonics
 Mercury
 Geomorphology
 Tidal despinning

ABSTRACT

Mercury's northern smooth plains are volcanically emplaced units characterized by ghost craters, volcanically buried impact basins, and thrust fault-related landforms. We analyzed the thrust fault-related landforms, traditionally categorized as lobate scarps and wrinkle ridges, within the northern plains in order to describe trends in how these landforms are organized and oriented and what style of deformation (either thin or thick-skinned) their map patterns represent. Our analysis also establishes geologic constraints for which global processes may have produced stresses contributing to these tectonic patterns. We mapped 4853 thrust fault-related landforms in the northern plains at a map scale of 1:1,000,000 using three MErcury Surface, Space, ENvironment, GEochemistry, and Ranging (MESSENGER) global monochrome mosaics. These landforms, described as curvilinear asymmetric ridges, frequently occur in complex geometrical arrangements that are interpreted to share similar structural characteristics. We called these arrangements "compound landforms". Like prior studies, we observed thrust faults to follow rims of buried craters. We also observed (1) sigmoidal rises bounded by fault-related landforms, (2) V-shaped rises composed of two landforms terminating at a single sharp point, (3) broad arcuate rises of nearly equal width, (4) parallel, evenly-spaced ridges, and (5) landforms showing alternation in direction of tectonic transport along strike. Respectively, we interpreted these landforms as transpressional uplifts, faults with sharply juxtaposing ramps, pop-up structures, fold and thrust belts, and antithetic fault intersections. By comparison with Earth analogues and patterns produced in numerical and physical models, our results suggest that deformation in the NSPs is thin-skinned. Orientation analysis showed that the northernmost landforms (90°–70°N) were predominantly oriented east–west while most of the landforms between 50° and 30°N were oriented north–south. Variations in orientation with latitude indicate that the growth of thrust fault-related landforms was influenced by sources of stress other than global contraction. If reorientation of the pole due to the formation of the Caloris basin impact did occur, the pattern of fault orientations indicates that geologic processes producing the pattern operated after reorientation.

1. Introduction

1.1. Overview of the tectonics of the northern smooth plains

Mercury's Northern Smooth Plains (herein referred to as the northern plains) is an expanse of smooth terrain volcanically emplaced (Head et al., 2011) through multiple phases of resurfacing events (Ostrach et al., 2015). The northern plains show very few superposing impact craters (Ostrach et al., 2015) and small, isolated regions of rough topography (Susorney et al., 2017). These plains embay heavily cratered terrain producing gradational to sharp physiographic boundaries (Denevi et al., 2013). The northern plains are abundant with ghost craters, volcanically flooded craters recognized by rings of tectonic

origin showing high topography likely localized above buried crater rims with lower topography interior to these rings, and volcanically flooded impact basins with rims jutting above the volcanic units (e.g. Freed et al., 2012; Klimczak et al., 2012; Watters et al., 2012). This suggests that heavily cratered terrain once extended up to the north pole, and then was buried by widespread effusive volcanism between ~3.7 and 3.9 Ga (Head et al., 2011; Denevi et al., 2013; Ostrach et al., 2015). As evidenced by the sharp contrast in the frequency of superposing craters between the northern plains and heavily cratered terrain, the northern plains are inferred to be younger than their underlying units. Regionally, the northern plains units are estimated to be ~1–2 km thick (Ostrach et al., 2015). The topography of the northern plains is 2 km below the global average elevation and shows lower

* Corresponding author.

E-mail address: kelsey.crane@uga.edu (K.T. Crane).

slopes than surrounding terrains (Zuber et al., 2012). This region also contains a ~950 km diameter topographic rise, commonly referred to as “the northern rise”, that stands ~1.5 km above the surrounding terrain (Zuber et al., 2012).

In addition to fresh and buried impact craters, thrust fault-related landforms are also prevalent in the northern plains (Byrne et al., 2014). These thrust fault-related landforms have traditionally been categorized into three groups based on morphology (Strom et al., 1975; Dzurisin, 1978; Watters, 1988; Watters et al., 2004, 2009 and many others): wrinkle ridges, lobate scarps, and high relief ridges. Wrinkle ridges have often been observed as anastomosing, arcuate, asymmetric ridges. They are interpreted to be anticlines above blind thrust faults, but for many of these landforms, a surface breaking fault is visible (Watters, 1988; Golombek et al., 1991; Schultz, 2000; Walsh et al., 2013; Watters et al., 2015a). They are more commonly observed in younger volcanic plains than heavily cratered terrains on Mercury and other bodies (Strom et al., 1975; Watters, 1988; Golombek et al., 2001) and are distinguished from the other common thrust fault-related landforms on Mercury, lobate scarps and high relief ridges, by their complicated, sinuous morphology. In contrast, lobate scarps are linear to arcuate asymmetric ridges with a fault trace intersecting the surface immediately in front of the steeper slope. High relief ridges are symmetric in cross section and rare compared to the previously discussed landforms. They are interpreted to be anticlines overlying high-angle reverse faults.

Although their individual morphologies (e.g. Watters, 1993) have been qualitatively described, wrinkle ridges, lobate scarps, and high relief ridges are not discrete, clearly distinguishable landform types. End member-type landforms that fit previous descriptions do exist as exemplars within each category, but we observe the vast majority of thrust fault-related landforms within the northern plains to exist on a spectrum between these three groups. Furthermore, classification of landforms as wrinkle ridges or lobate scarps does not facilitate the mapping process or our understanding of how the underlying structures form and link. Thus, we do not attend to the traditional terminology, similar to the approach taken by Byrne et al. (2014), and do not categorize our mapped thrust fault-related landforms in the traditional sense. Rather, we map fault surface breaks and anticline crests and identify isolated landforms, referred to as thrust fault-related landforms and larger, more complex landforms, referred to as compound landforms from hereon. Compound landforms consist of geometrically related anticlines and traces that, by comparison with analogues, are interpreted to share a structural relationship. In using a single term to describe the landforms, most of these landforms would have been classified as wrinkle ridges, and the detail of their structure would have been lost.

Thrust fault-related landforms in the northern plains on Mercury have not previously been mapped in sufficient detail to describe map patterns and regional trends in landform morphology and orientation. Detailed morphological descriptions, identification of map patterns, and structural interpretations of these landforms can constrain their subsurface fault architecture, thickness and geometry of the plains deposits, and details of the global or regional processes associated with their formation.

In particular, observational and statistical analyses of morphologies and map patterns and comparison of landform characteristics with planetary analogues could suggest whether faults below northern plains structures are confined within the volcanic plains units or whether they root deeper into the subsurface. Based on results from elastic dislocation modeling and comparison with Earth analogues, Watters (2004) proposed that thrust faults in the Martian plains shallowly root into upper volcanic units. Other studies have also suggested that ridges on Mars are underlain by faults that penetrate primarily upper units and regolith, evidenced by modeling, landform geometry, and again, the resemblance of these structures to terrestrial landforms (e.g. Plescia and Golombek, 1986; Watters, 1988; Mangold et al., 1998). Comparisons to

terrestrial landforms indicate that structural styles in these terrains are similar to thin-skinned tectonics on Earth. For example, the Yakima fold and thrust belt in the Columbia Plateau of eastern Washington has been suggested as an analogue to thrust fault-related landforms in flood basaltic units on Mercury, the Moon, and Mars due to their basaltic composition, systems of parallel ridges, and low-lying, only slightly deformed regions between those ridges (Plescia and Golombek, 1986; Watters et al., 2004). The faults underlying this thrust belt shallow into a décollement less than 10 km below the surface (Casale and Pratt, 2015).

In contrast, Peterson et al. (2017) contend that northern plains thrust faults extend deeper into regolith and cratered units underlying the plains because elastic dislocation modeling results best produced observed topography when model faults are deep-seated. Similar conclusions have been drawn by Schultz (2000), Golombek et al. (2001), and Montési and Zuber (2003) for thrust fault-related landforms on Mars based on kinematic model results best resolved by faults that do not shallow into décollements and spatial and topographical relationships between parallel landforms which could result from deeply rooted faults. A similar deformation style to that suggested has been observed on Earth in the Rocky Mountains of Wyoming, and is called thick-skinned tectonism, in which thrust faults extend down to a crystalline basement (e.g. Pfiffner, 2017). Landforms like the Wind River thrust fault share similar topography and length relationships to thrust fault-related landforms on Mercury (Watters and Robinson, 1999), and thus can be suggested as analogues to northern plains thrust fault-related landforms. Contrasting analogues and a lack of detailed mapping have limited consensus for the depth of faulting underlying the northern plains structures.

1.2. Tectonic processes and associated stress states on Mercury

The tectonics of Mercury have been influenced by many global and regional processes, including impact cratering, tidal despinning, cooling, subsidence, and changes in orbital parameters that lead to differential surface temperature conditions and changes in solar tides. Each of these processes induces a unique set of stresses within the lithosphere. Impact shock waves propagate from the location of impact and excavate rock, producing the negative topography associated with impact craters (Melosh, 1989). For the remainder of these processes, the orientations and magnitudes of the principal stresses control whether the lithosphere experiences permanent strain and, if so, whether it is accommodated by shortening or extension. To produce faults, principal stresses must be compressive in all orientations (vertical and horizontal) and be of sufficient difference to one another to overcome the strength properties of the host rock. The orientation of the intermediate principal stress determines the 3D geometry of those faults (Anderson, 1951; Jaeger et al., 2007). Once a fault has formed, it may continue to grow or new similarly oriented faults may propagate until the directions of stresses change or until stresses are no longer sufficiently large to promote failure.

Impact cratering and global cooling are the geologic processes that likely operate over the longest time-scales on Mercury. During the first ~0.5 Ga of solar system history, impacts were more frequent and destructive due to a more substantial population of impactors and a higher concentration of larger-bodied impactors within that population (Marchi et al., 2013). These impacts drove the formation of impact craters and basins, which have degraded over time (e.g. Fassett, 2012; Kinczyk et al., 2016). Global cooling would have prompted global contraction, that is found to have led to widespread thrust faulting with increased activity early in Mercury's history that slowed down substantially by ~3 Ga (Banks et al., 2015; Crane and Klimczak, 2017). Stresses from global contraction are estimated to be horizontally isotropic, and therefore, if large enough, these stresses should have formed a planet-wide distribution of randomly oriented thrust fault-related landforms (Solomon, 1976, 1978; Watters et al., 2001, 2004).

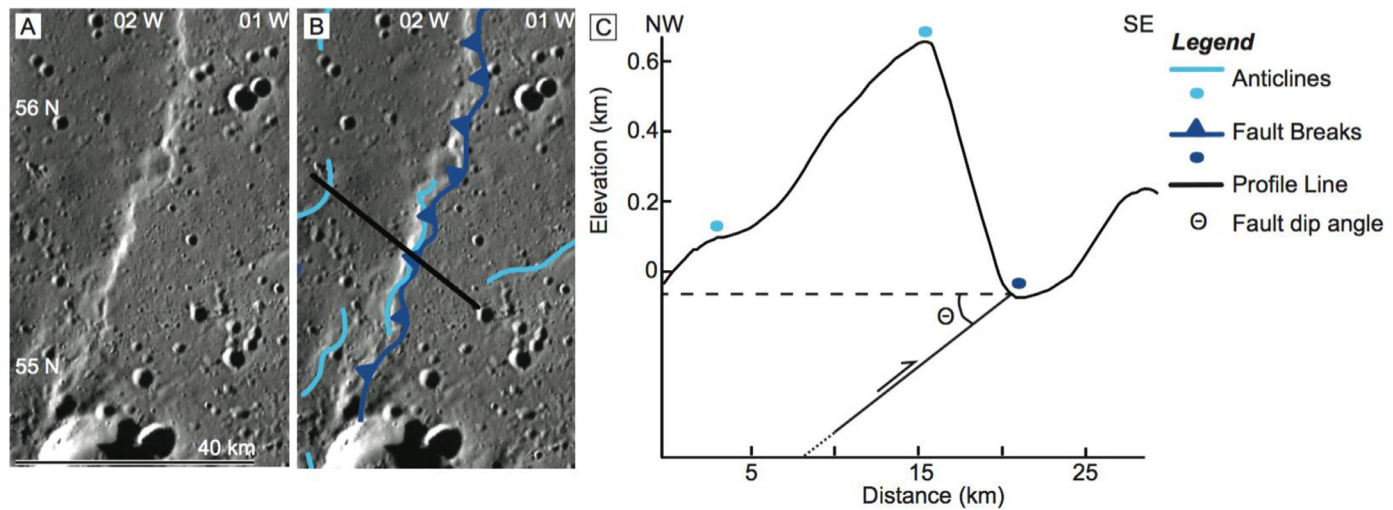


Fig. 1. This figure shows an example of the thrust fault-related landforms mapped in this study. (A) The bright, sharp contrast between the westward-dipping scarp and the flat, eastern terrain indicates that a fault surface break is likely present. The rounded, high topography above the break, along with three additional topographic rises without apparent scarps, were recognized as anticlines. Using traditional terminology, this landform would be classified as a lobate scarp. (B) The fault break and associated anticlines (light blue) are shown at 1:1,000,000 scale, the same scale at which we viewed them during mapping. The triangles on the dark blue fault trace line indicate the dip direction of the underlying fault. Both (A) and (B) are images from the MDIS monochrome global mosaic, shown in orthographic projection centered at 0°E, 5°N. The black line crossing (B) corresponds to the profile line shown in (C). (C) MLA-derived topographic profile across the structure with 21 times vertical exaggeration, showing a shallowly dipping back slope and steeply dipping scarp associated with the landform. Light and dark blue dots indicate where anticlines and fault were mapped on the image. Thrust faults interpreted to underlie these landforms may or may not break the surface, but they dip in the direction of the shallow slope (e.g. Watters, 1988). (For interpretation of the references to color in this figure legend, the reader is referred to the web version of this article.)

Dzurisin (1978) and many others after have observed that the tectonic patterns on Mercury are not random, and so other sources of stress must have contributed to the observed landform types and orientations.

Tidal despinning, subsidence, reorientation, and changes in orbital parameters lead to different stress states in the lithosphere than those caused by cooling and crystallization in the interior of Mercury. Therefore these processes may have exerted some influence on the pattern of landforms in our study area. A tidal despinning pattern, in particular, has been proposed for Mercury (Melosh and Dzurisin, 1978; Dombard and Hauck, 2008; Matsuyama and Nimmo, 2009; Beuthe, 2010). When operating in isolation, tidal despinning is predicted to cause tensile stresses at the poles that when interpreted with Anderson's Theory of Faulting (Anderson, 1951) are predicted to cause circumpolar graben (Melosh, 1977; Pechmann and Melosh, 1979; Beuthe, 2010) but when assessed with failure criteria, they are found to produce a random set of joints (Klimczak et al., 2015).

The geologic history of Mercury can be interpreted by establishing the relative timing of these processes. Thrust faulting resulting from global contraction is estimated to have begun as early as ~3.9 Ga (Crane and Klimczak, 2017) near the time of the Caloris impact (Spudis and Guest, 1988). Reorientation caused by the Caloris impact could have only happened after the formation of the Caloris basin. Some studies conclude that tidal despinning must have predated northern plains emplacement and reorientation (e.g. Pechmann and Melosh, 1979) while others suggest that reorientation preceded tidal despinning (e.g. Matsuyama and Nimmo, 2009). Large horizontal compressive stresses from global contraction are estimated to have counteracted stresses that would have otherwise caused opening-mode fractures and normal faulting due to despinning and reorientation (Dombard and Hauck, 2008; Beuthe, 2010; Klimczak et al., 2015). Opening mode fractures themselves facilitate the transport of volcanic materials to the surface to form the plains, and these materials must have been present to induce subsidence. With a well-established age for the northern plains, the map patterns of shortening landforms within its borders could establish the relative timing of tidal despinning, pole reorientation, and global contraction.

1.3. Goals of the work

Thrust fault-related landform morphologies and map patterns within the northern plains have yet to be described in detail using MErcury Surface, Space, ENvironment, GEochemistry, and Ranging (MESSENGER) datasets. Analyses and descriptions of the morphology of the landforms can indicate the style of deformation within the northern plains: either thick- or thin-skinned, with faults extending below the northern plains or shallowing at the base of these volcanic units. It is also possible to describe geologic controls on the strike (orientation), sinuosity, breadth, and depth of faulting by characterizing these morphologies and when possible, relating them to Earth analogues. The aim of this work is two-fold:

- (1) Describe the common shortening-related landform morphologies and their map patterns within the northern plains and discuss their implications for deformation styles and subsurface fault geometry.
- (2) Assess combinations of geologic processes which either contemporaneously, temporally overlapping, or in succession could have produced stresses that, if great enough in magnitude, could have contributed to the observed tectonic patterns.

2. Methods

2.1. Identification, mapping, and interpretation of thrust fault-related landforms

Using MESSENGER photomosaics and topographic data, we mapped landforms, including faults with clear surface breaks and broad ridges with no clear surface breaks interpreted to be anticlines, at the 1:1,000,000 scale. All thrust fault-related landforms with any component of their length extending into the northern plains were included in our mapping process. Faults were mapped where a clear transition was observed between a steep scarp and what can be interpreted to be the fault footwall. These transitions are often linear and sharp, possibly indicating a fault surface break. When the contact is less

morphologically crisp, but the sense of asymmetry along the ridge was apparent, we interpret a fault must be present (Fig. 1). The direction of more gradually increasing elevation across the ridge was interpreted to be the direction of tectonic transport, or vergence. When landforms occurred in linear arrangements, such as en echelon segments or multiple surface breaking faults below a single anticline, a network number was assigned to each fault or anticline within the arrangement to indicate that they belong to a group. Each fault was then assigned an identification number. When crests of anticlines were adjacent to a fault trace such that they clearly belonged to the same structure, they were mapped and labeled with the same identification number as the associated fault. When multiple anticlines were associated with a single fault trace, all associated anticlines were assigned the same identification number as the corresponding fault. When multiple fault surface breaks were visible below a single anticline, the anticline was assigned the same identification number as the longest adjacent fault trace. Anticlines not associated with surface-breaking faults were assigned a unique identifying number.

We took three additional precautions to lessen uncertainty associated with mapping. First, we mapped anticlines and fault surface breaks as polylines in ArcMap using the streaming function, which automatically produced equally spaced nodes along each polyline. The projection and center of projection used can also greatly affect the accuracy of the mapping process. The northern plains were divided into $10 \times 10^\circ$ bins, and the center location of each bin was used as the center of an orthographic projection of the mosaics and hillshades. This minimized mismatch between the imaged landforms and the polylines we drew to indicate their locations. All landforms within each bin were mapped before the projection was changed to center upon the next bin. Finally, we utilized multiple mosaics and thus illuminations in the mapping process: the Mercury Dual Imaging System (MDIS) MESSENGER global mosaic basemap data record (version 1), eastern illumination mosaic, and western illumination mosaic (all 166 m/pixel). When observing our mapping locations, we viewed each mosaic separately, determined which mosaic displayed the best viewing and illumination geometries to highlight the landforms, and used that mosaic in mapping. Occasionally, some landforms could be observed in one mosaic, but not in the other two. When this occurred, multiple illumination mosaics were used consecutively to capture all landforms in our map. These mosaics were supported by hillshades with multiple illumination conditions created from the Mercury MESSENGER Mercury Lazer Altimeter Digital Elevation Model (MLA DEM, 665 m/pixel, Zuber et al., 2012). Using a DEM facilitated the recognition of landforms during mapping.

2.2. Identification, mapping, and description of compound landforms

Once all landforms were mapped, each bin was visually assessed for trends in map patterns and in morphology associated with those landforms. During the initial mapping process, the entirety of each bin was not visible at the 1:1,000,000 scale, and therefore, the connectivity of landforms across multiple bins or even across longer distances within the same bin was not apparent during the mapping process. However, upon increasing our scale of view, we were able to describe compound landforms. Whereas an individual landform may not link to any other landforms, the morphology of compound landforms and the geometry of their associated map patterns allow us to interpret the faults and/or anticlines to be structurally related based on comparison with terrestrial and planetary analogues. In each bin, observations of compound landforms and other structural patterns were recorded. Our descriptions included size (where we could confidently take measurements because the landform had not been too degraded or reshaped by impacts), shape, position, relationship to topography, relationship to gravity (where Earth analogues prompted that this property should be investigated), and spatial relationship to other compound landforms and the northern plains boundaries. After all bins had been assessed, we

reviewed our observations for patterns, for compound landforms and/or landform characteristics that were observed multiple times across the northern plains.

Identifying Earth and other planetary analogues for compound landforms and the structural characteristic was an iterative process. Detailed descriptions for each of the compound landforms were composed first, and then extensive literature searches for key terms within the descriptions were conducted. Once potential analogues were identified, we scanned the examples within the literature for descriptions of morphology and setting. These descriptions and accompanying images were compared to our observations of landforms on Mercury. We also searched for the analogues described in the literature using Google Earth Pro, and compared satellite images from Earth to our Mercury mosaics. When key characteristics from potential Earth analogues differed from our observations, we searched the literature for sandbox and computer models that generated landforms with similar morphology and/or tectonic pattern. For some compound landforms, model parameters that caused morphological variations from the previously investigated Earth analogues were able to accommodate the observed differences between our compound landforms and the analogues. After locating analogues that reflected our observations of Mercury, we searched within the literature for proposed structural interpretations and subsurface geometry of those landforms. We purposefully conducted this portion of the literature review second so that the process of identifying analogues was not biased by our preconceptions of what the depth and style of faulting in the northern plains might be.

3. Map and landform description

In total, we mapped 2053 scarps with surface breaks and clear directions of vergence and 2800 anticlines within the northern plains (Fig. 2, included as a supplementary shapefile). The longest mapped fault surface break was ~ 255 km and the shortest was ~ 3 km. The longest mapped anticline was 211 km and the shortest mapped anticline was ~ 3 km. We identified 218 linear to curvilinear groups of landforms, such as en echelon fault-related landforms or multiple anticlines along a single fault trace. The cumulative lengths of fault surface breaks and anticlines were 61,265 km and 72,336 km, respectively. Five common compound landforms and one common structural characteristic were identified in our analysis. The compound landforms described are observed in isolation and transitioning into one another, and therefore imply complex structure like that observed on Earth and other planets.

Below we describe in detail (1) number and dimensions of identified compound landforms for which we felt accurate measurements could be taken, (2) the morphologies and map patterns of the compound landforms, (3) analogues to the compound landforms observed, and (4) the structural interpretation of those analogues and their implications for landform development on Mercury. The locations of these landforms are included as a supplementary shapefile.

3.1. Faults following crater rims

We identified 429 circular rings of thrust fault-related landforms (e.g. Fig. 3). For 422 of these landforms, we measured the diameters of the rings using the geodesic length tool in ArcMap. These values range from 5 to 589 km. We observe an abundance of smaller diameter rings and progressively fewer large diameter rings. We calculated the mean diameter to be 38.1 km, the median to be 24.5 km, and the standard deviation to be 46.7 km. The observation of skewed diameter distribution is supported by the slope (~ -3.3) of the cumulative frequency distribution of diameters, which is in agreement with calculations of crater distributions for young surfaces on Mercury (Strom et al., 2011). Although there is a wide variation in diameter, we do not observe or record wide variation in elevations associated with these rings.

Each ring is composed of varying numbers and lengths of fault

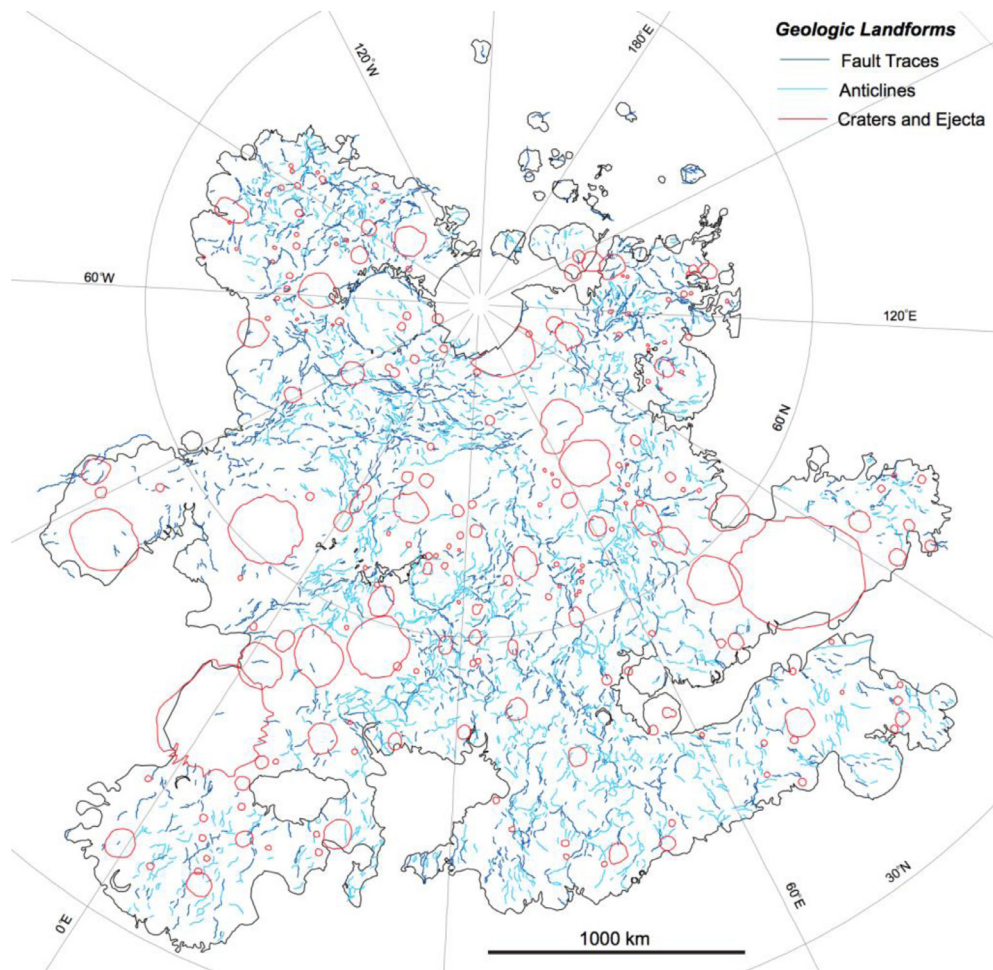


Fig. 2. This map displays the thrust fault-related landforms we identified in the northern plains (black outline) and mapped on a scale of 1:1,000,000. The nearly 5000 structures are shown in blue, and areas superposed by craters and crater ejecta are outlined in red (Denevi et al., 2013). Map is shown in stereographic projection centered at 30°E, 66°N. (For interpretation of the references to color in this figure legend, the reader is referred to the web version of this article.)

traces and anticlines. When rings of landforms with visible fault surface breaks are observed, faults typically verge outward from the center of the ring implying that their slip surfaces dip toward the center of the buried crater. Anticlines are distinguishable from buried crater rims by their symmetry and pronounced topography. Smaller rings (< 15 km) are often composed of a single, curved anticline. Moderately sized rings (15–100 km) typically include a combination of fault traces and anticlines. For example, in Fig. 3, at least four rings each ~ 50 km in diameter can be seen. One of these example rings (labeled “1”) is entirely composed of anticlines, two are produced by a combination of anticlines and fault traces (labeled “2” and “3”), and a fourth is a nearly

complete ring of surface breaking faults (labeled “4”). The largest mapped rings (> 100 km) are outlined by multiple fault traces and anticlines, which are sometimes arranged in en echelon patterns. Landforms surrounding larger rings do not appear longer or to have more associated topography than those associated with smaller rings. Rings of all diameters are observed in each of the analyzed bins, and are very common throughout the plains except in regions interpreted to be floors of large impact basins.

These rings were previously described as wrinkle-ridge-rings—landforms that follow the rims of buried impact craters. Wrinkle-ridge-rings have not only previously been observed on Mercury (Freed

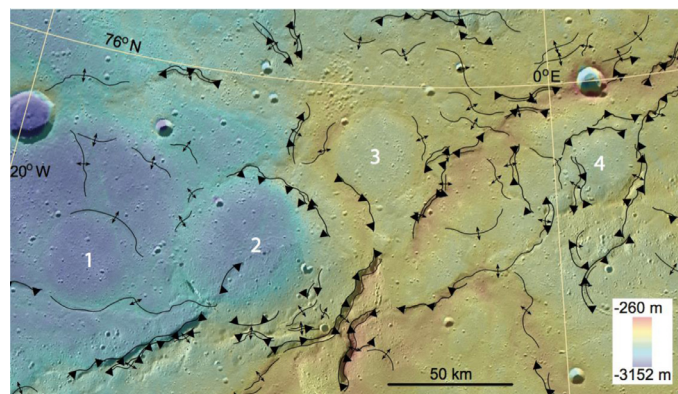


Fig. 3. Four buried impact craters marked by thrust fault related landforms are highlighted in this MDIS monochrome global mosaic overlain with MLA topography. These examples display the breadth of ways in which shortening landforms outline buried impact craters. The mosaic is shown in orthographic projection centered at 74°N, 4°W.

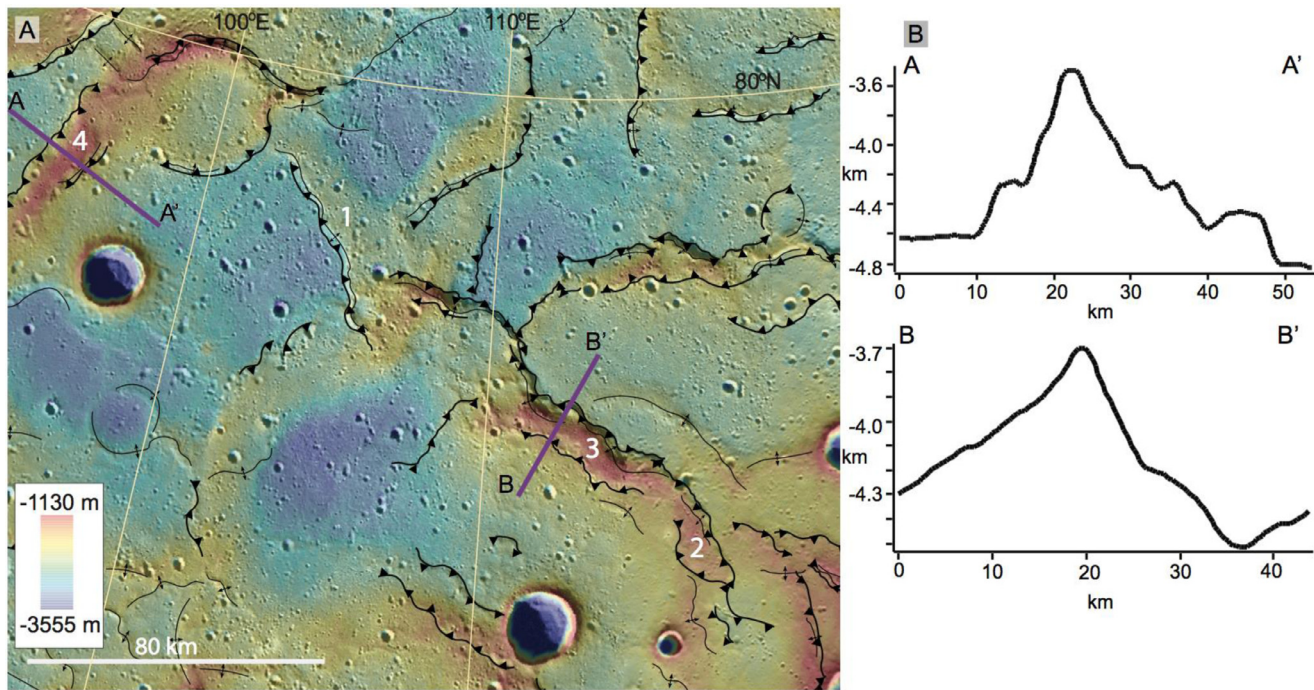


Fig. 4. Examples of broad, equal-width rises in a linked arcuate network with topographic profiles corresponding to two rises in the image. Structural mapping shows that some rises are bounded by two outward verging thrust fault-related landforms, while others are only clearly bounded on one side. (A) A section of one of these networks just south of Yoshikawa crater is shown in an MDIS monochrome global mosaic overlain with MLA topography in orthographic projection centered at 79°N, 114°E. Profile lines are shown in purple. (B) Topographic profiles with $\sim 20\times$ vertical exaggeration corresponding to lines A-A' and B-B' show that these landforms are approximately symmetric compared to other thrust fault-related landforms and have distinct peaks. (For interpretation of the references to color in this figure legend, the reader is referred to the web version of this article.)

et al., 2012; Klimczak et al., 2012; Watters et al., 2012; Wright et al., 2018), but also on Mars (Watters, 1993; Neel and Mueller, 2007), and the Moon (Wood et al., 2005; Byrne et al., 2015). Similar to rings on other bodies, the wrinkle-ridge-rings on Mercury are characterized by broad topographic depressions within the more elevated rims (Freed et al., 2012). They have also been observed to host graben interior to the ring (Klimczak et al., 2012; Watters et al., 2012) and more rarely, to be bounded by graben rather than thrust fault-related landforms (Klimczak et al., 2012).

Schultz (2000) as well as Allemand and Thomas (1995) suggest that the rims of impact craters act as stress concentrators. The effectiveness of concentration was estimated in these studies by comparing crater rims to punched holes in metal sheets, which were then stressed. Comparing impact craters to notches rather than holes, it is possible that stresses are three times as great or more at the base of a bowl shaped crater than within the terrain surrounding the crater. Studies of stress concentrations along notches with level basins suggest that craters with more subtly concave floors (e.g. flat-floored craters) concentrate stresses closer to their rims (Young and Budynas, 2002). If faults are produced by stress concentrations along craters, faults should root near the center of crater floors or crater floor-wall contacts and verge outward, away from the crater center. Models specific to Mercury (those discussed in the previous paragraph) also show that stronger volcanic units that overly weaker crustal layers, thinning of volcanic units over rims, and thinner crustal units such as volcanic units within impact craters concentrate stresses within crater rims to five times the level in plains exterior to those rims.

Faults tend to propagate along favorably oriented pre-existing weaknesses (e.g. Cowie and Scholz, 1992; Vermilye and Scholz, 1998; Jaeger et al., 2007). Faults may use the boundaries between crater fill, floor, and walls as pre-existing weaknesses along which to propagate. We acknowledge that faults bounding larger basins such as Mare Crisium on the Moon have been found to verge inward toward the crater

center, but these faults are predicted to utilize the boundary between the crust and uplifted mantle as a pre-existing weakness (Byrne et al., 2015). Buried craters within the northern plains are not as large as the basin hosting Mare Crisium and the faults at these craters are not likely associated with mantle uplift, such as suggested for those in Mare Crisium. We interpret the uniformity of topography despite the variability of associated crater diameter to be a consequence of larger craters lacking substantially larger depth to diameter ratios than smaller craters and level floors. Thus, faults associated with larger craters may not reach depths substantially deeper than faults propagating through smaller craters.

3.2. Broad, linear to arcuate rises of equal width

Networks of broad, linear to arcuate rises bounded laterally by thrust fault-related landforms verging away from the rise are observed near regions with an increased density of impact related landforms throughout the northern plains. Of the 71 landforms we identified, 44 were measured because they have both clear lateral boundaries, such as where a steep scarp face sharply met more gentle terrain, and locations where the lengths of the rise terminated, lost topography, or transitioned into another landform are visible. The lengths of measured landforms are widely distributed with a mean of 50.7 km and standard deviation of 35.6 km. The widths, however, are more narrowly distributed with a mean of 12.6 km, a median of 10.7 km, and a standard deviation of 7.5 km. For example, two of the longest rises (measuring 100 and 111 km) have widths of 9.5 and 9.3 km. The longest rise (146 km long) has a width of 39.5 km, but this landform is much wider than all others we observe.

Rises link and terminate into each other and into other landforms, producing their networked structural patterns. Gradational, sometimes arcuate transitions link multiple rises. Where rises meet flooded or buried craters, four different transition morphologies are observed: (1)

the rise ends abruptly along the rim of the crater; (2) one of the two bounding thrust fault-related landforms links to a through-going landform within the crater; (3) the rise itself follows the crater rim curving through the crater interior and continuing beyond the other side of the crater or (4) one of the two landforms links to a wrinkle-ridge-ring. In cases (2) and (4), small en echelon anticlines indicate stepover regions between the two landforms. Each case is exemplified in Fig. 4, and the landforms are labeled with corresponding numbers.

We interpret the broad rises to be pop up structures. Due to their consistent width throughout the northern plains, it is likely that the structures root into the same layer or have similar depth extents. Assuming fault dips of 60, 45, 30, or 20°, the depth of that layer would be ~9, ~5, ~3, or ~2 km respectively. These depths are somewhat larger but of the same order of magnitude as the estimated depths of the volcanic units of the northern plains. Pop up networks, such as the Mari Bugdi Pop Up Zone within the Sulaiman Fold and Thrust Belt, have also been shown to root into a single layer and to dip as steeply as 60° (Jadoon et al., 1994). In this zone, passive roof deformation generated pop ups solely within geologic units above one specific décollement. By analogy, the proposed pop up networks in the northern plains could root into the base of the northern plains volcanic units.

3.3. V-shaped rises

Twenty V-shaped rises are observed in groups within the northern plains. All groups are north of 70°N or south of 40°N. The landforms are composed of two thrust fault-related landforms meeting at a sharp intersection point (e.g. Fig. 5). The landforms verge away from the central angle between the two landforms, and the bisector of the angle is typically oriented to the north. The back limbs of the two landforms are often characterized by anticlines in smaller structures (~10 km across the widest span of the "V") and both anticlines and plateaus in larger structures (~150 km across the widest span of the "V"). The highest topography along the rise occurs at the landform intersection point. In larger structures, a small plateau can be observed at this intersection interior to the central angle. For example in Fig. 5, the westernmost V-shaped rise has a small plateau visible within the central angle, while the southernmost rise does not. Away from the vergence direction, the landform elevation gently tapers off.

We suggest two possible formation mechanisms for these landforms. One possibility is that two independent faults grew towards each other and their growth along strike ended once they linked. Anticlines

developed above the faults as they propagated. Typically though, linkage is characterized by restraining bends and stepovers—landforms that tend to be more arcuate than the crisp intersection points observed (e.g. Mann, 2007). A second possible mechanism is that as a single fault grew it was deflected or redirected along strike. Impact craters, basins, and/or pre-established fault systems could cause this redirection. A similar landform, the Horse Heaven Hills Anticline, is observed within the Yakima Fold and Thrust Belt (YFTB, Fig. 5B), a set of terrestrial thrust fault-related landforms within the Columbia River flood basalts. This anticline was likely redirected along the Olympic Wallowa Lineament (OWL) and pre-existing Wallowa Fault (Casale and Pratt, 2015). A separate study suggested that the termination and redirection of the YFTB landforms was caused by both the presence of the OWL and the gravity low associated with the Pasco basin (Blakely et al., 2014). We analyzed the locations of V-shaped rises in relation to the free air gravity anomaly field of Mercury (Mazarico et al., 2014). In some cases, such as those shown in Fig. 5A, large V-shaped rises terminate along the edge of gravity lows. By analogy to the YFTB landforms, these may form as a consequence of relatively thin-skinned deformation as underlying thrust faults follow a décollement horizon between 5 and 10 km depth (Casale and Pratt, 2015).

3.4. Sigmoidal rises

We observe 19 lense or sigmoidal shaped rises bounded by thrust fault-related landforms verging outward from the center of the rise. We felt confident to take measurements for 10 of these sigmoidal rises. They have an average length-to-width ratio of ~3.3 and ranged in length from ~10 km up to ~200 km. Larger rises are characterized by clearly identifiable fault surface breaks along their boundaries and plateau like uplift within these boundaries. For example, in Fig. 6 the sigmoidal rise shown has a 21 km plateau bounded between oppositely verging thrust faults. Additional faults and/or anticlines cross cut through the plateau, frequently occurring sub-parallel to one of the bounding landforms. Within the plateaus, it was also common to find linear, narrow landforms connecting to one another at irregular angles with no apparent planimetric geometric relationship to the bounding faults. Arrows in the figure point to two examples of these smaller interior landforms. Smaller rises were smooth within their interior. Both large and small rises were more common south of 80°N.

We interpret large sigmoidal rises to be stepovers, zones of slip transfer between faults, and smaller sigmoidal uplifts to be restraining

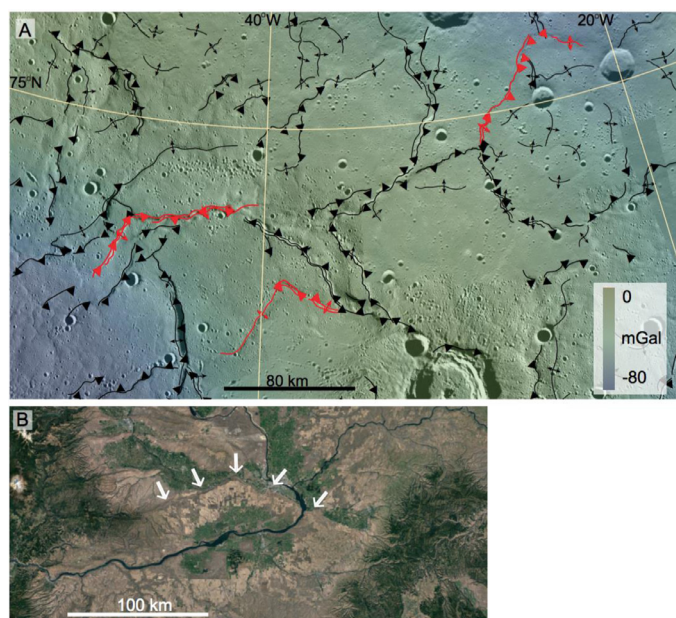


Fig. 5. V-shaped rises composed of two landforms terminating at a single point. (A) Three examples are highlighted with red symbology on an MDIS global mosaic overlain with the free air gravity anomaly field (Mazarico et al., 2014). Structural interpretations show that one of the two adjoining landforms in each example terminates near a negative gravity anomaly. The mosaic is centered at 73°N, 46°W in orthographic projection. (B) A Google Earth image of the Horse Heaven Hills anticline, a possible Earth analogue, clearly displays a similar V-shaped morphology. The anticline limbs and intersection point of the landforms composing its limbs are indicated with white arrows. (For interpretation of the references to color in this figure legend, the reader is referred to the web version of this article.)

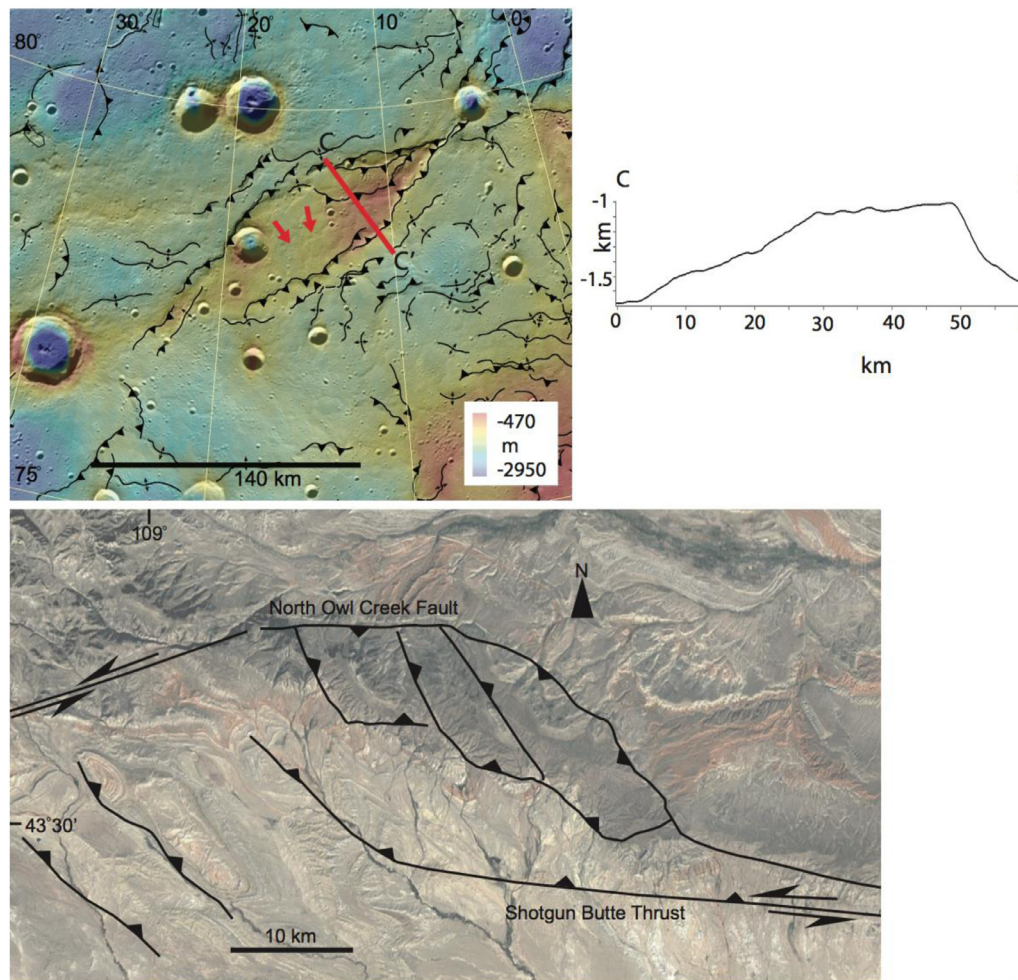


Fig. 6. Example of a large sigmoidal rise in the northern plains with a possible Earth analogue to this rise. (A) This 200 km long rise is displayed in an MDIS global mosaic overlaid with MLA topography using an orthographic projection centered at 78°N, 15°W. Structural interpretation indicates that the rise is bounded by thrust fault-related landforms verging away from the center of the rise. (B) Similarly, the Owl Creek Pop Up Structure, shown in a Google Earth image overlaid with structural interpretation (Paylor and Yin, 1993), shows a map pattern of thrust faults verging outward from the center of the rise and interior landforms subparallel to one of bounding landforms. (C) Rises are also both characterized by a plateau, shown here in a topographic profile with ~11x vertical exaggeration taken across the sigmoidal rise shown in (A). The profile line corresponds to the red line in (A). The plateau has ~1 km of relief and is ~20 km wide. (For interpretation of the references to color in this figure legend, the reader is referred to the web version of this article.)

bends, jogs along the length of a fault which concentrate horizontal compressional stresses (Mann, 2007). Both landforms are associated with fault slip in the direction of strike, however, these landforms may be indicative of oblique rather than pure strike-slip motion. Massironi et al. (2015) identified similar landforms in the mid-latitudes on Mercury and thoroughly described common strike slip kinematics on the planet. They do not identify any sigmoidal rise as large as the example shown in Fig. 6A. If this structure does imply oblique slip, then that slip predates the emplacement of the craters on both ends and interior to the structure. These craters do not display evidence of strike-slip.

Large stepovers like the one shown develop as two faults grow towards each other. Modeling shows that parallel anticlines and small polygonal shears develop in the interior of the rise when relatively little overlap exists between the fault tips before linkage (McClay and Bonora, 2001; Mitra and Paul, 2011). Both interior anticlines and shears are observed within two large stepover structures identified ~75°N. This style of linkage is similar to the Owl Creek Pop Up Structure near Laramie, WY (Fig. 6C). Here, the Shotgun Butte Thrust and North Owl Creek Fault transfer shortening between two low-angle thrust systems. Three sub-parallel anticlines cross cut the rise (Paylor and Yin, 1993). Although it is unclear how deep these low angle faults root, they are projected to just over 1 km in cross sections produced by Paylor and Yin (1993), and steeply dipping faults are only locally produced and necessary to produce the pop up between the two low angle thrusts.

3.5. Evenly-spaced parallel ridges

The final type of thrust fault-related compound landforms that we identify within the northern plains is parallel, evenly spaced topographic highs. We located 26 sets of three or more parallel ridges, and felt confident in measuring the characteristic lengths and widths of 22 of these systems of ridges. Width was recorded as the distance between the two ridges at either end of the systems. Although there is a wide distribution of lengths and widths, the ratios of length-to-width are approximately narrowly distributed and slightly skewed toward higher ratios with a mean of 2.8, median of 2.0, and standard deviation of 0.7. Short, narrow ridge systems are composed of parallel to subparallel anticlines. Longer, broader ridge systems contain parallel to subparallel anticlines and anticlines above fault traces, with all faults verging in the same direction and anticlines with the same sense of asymmetry. These individual landforms increase in elevation in the direction of vergence, regardless of whether their overall trend was linear or arcuate. In most cases, the ridges appear to have extremely smoothed topography, indicating that they may be older than other nearby landforms, but some, such as the Le Dauphine Rupes system have crisp morphologies with clear surface breaking faults, dramatically asymmetric slopes, and few superposing craters (Fig. 7). In Figs. 7A and C, we show a topographic profile and structural map of the Le Dauphine Rupes system where topography increases slightly to the northeast, the direction of vergence.

We interpret these systems of parallel ridges to be (1) fold and thrust belts in the case that the system is composed of linear ridges or (2) rings within or bordering ancient impact basins when the system is composed of arcuate ridges. Massironi et al. (2015) also classified the Le Dauphine

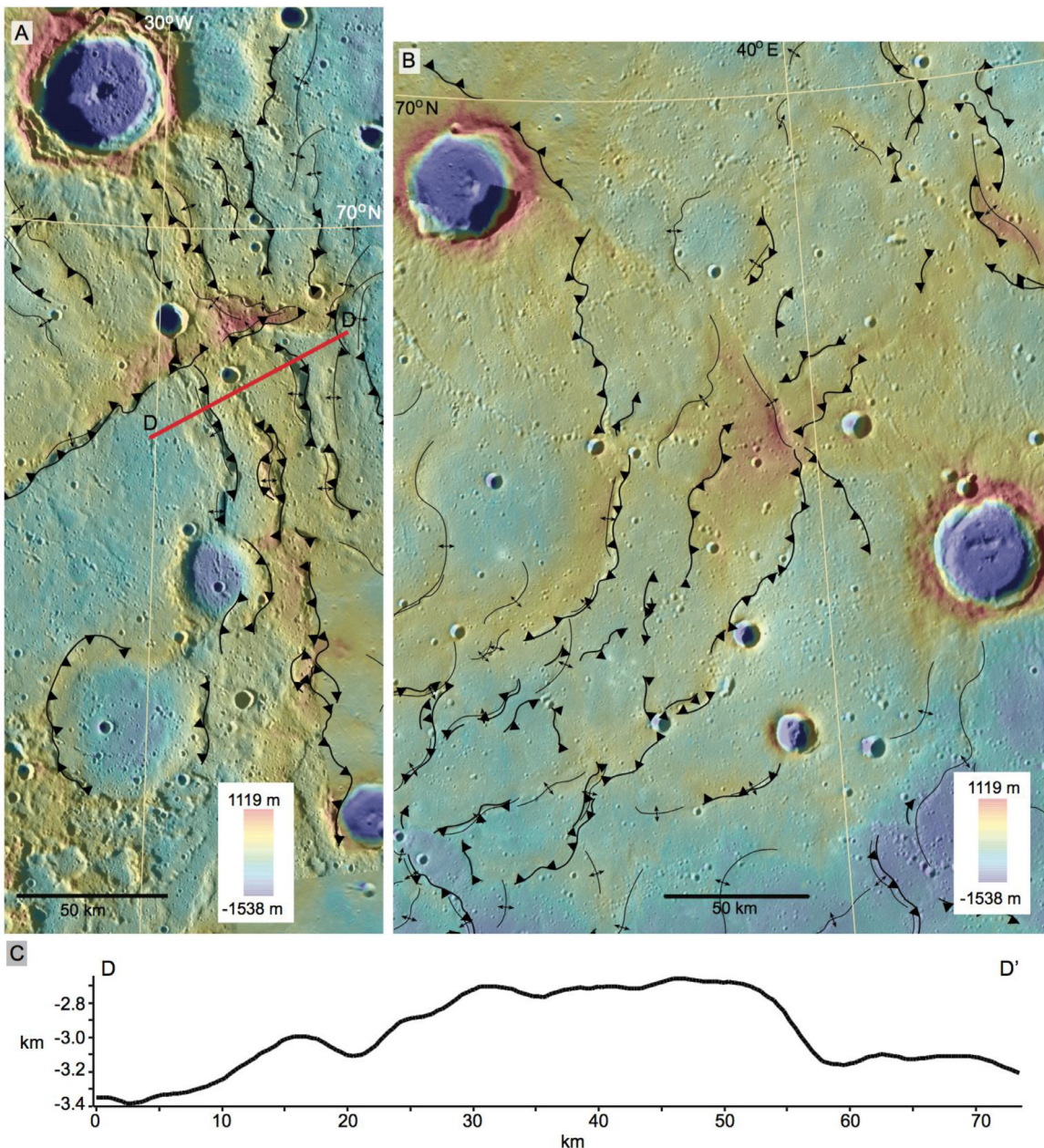
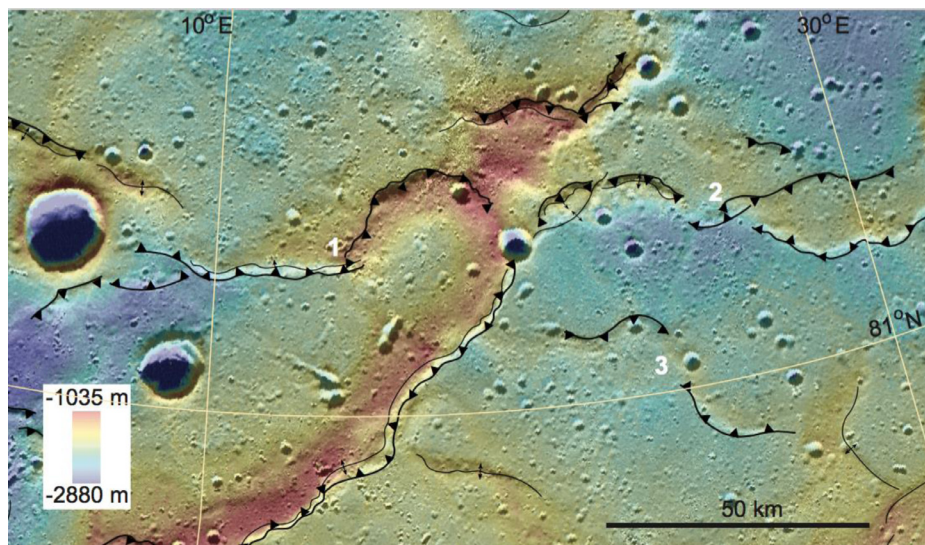


Fig. 7. Systems of linear parallel ridges. (A) The Le Dauphine Rupes fault system is shown in a global mosaic overlain with MLA topography in orthographic projection centered at 68°N, 28°W. Our structural mapping indicates that the landforms in this system verge to the northeast. The line across which we created a topographic profile is shown in red. (B) An unnamed fault system near Rivera crater exhibits a curvilinear plan form. This system is displayed with a global mosaic overlain with MLA topography in orthographic projection centered at 66°N, 35°E. The curved map patterns exemplify arcuate systems of parallel ridges. (C) This topographic profile with 14x vertical exaggeration was taken across the Le Dauphine Rupes fault system shown in (A). Topography associated with system extends for almost 50 km laterally and ~500 m vertically, and the profile rises in elevation to the right (East). (For interpretation of the references to color in this figure legend, the reader is referred to the web version of this article.)

Rupes system as a fold and thrust belt containing some transpressional landforms. Periodically spaced landforms, traditionally termed wrinkle ridges, have been recognized on Venus (Bilotti and Suppe, 1999), Mars (Montési and Zuber, 2003), Earth (Watters, 1989) and the Moon (Yue et al., 2015). Models suggest that evenly spaced thrusts resulting in evenly spaced ridges in fold and thrust belts correspond to rapid shortening rates (Couzens-Schultz et al., 2003). These rates produce narrow thrust sheets in which evenly spaced ramp anticlines propagate within a passive roof duplex. Strong décollements also promote foreland propagation of structures (Couzens-Schultz et al., 2003) where often topography increases into the foreland. The remarkably even spacing of these systems on Mercury resembles the faults of the upper

Lesser Himalayan Duplex. Long et al. (2010) proposed that the faults within this duplex root into a single shallow quartzite layer. Given that these landforms on Mercury are observed less often than other compound landforms, they may represent fault propagation through regions where thinner regolith underlies the northern plains volcanic units, and thus faults root to a stronger décollement. As most appear to be older landforms based on their heavy degradation, they may have formed soon after plains emplacement that coincides with the time when global contraction was operating at its highest resolvable rate (Crane and Klimczak, 2017).



3.6. Changes in vergence

Abrupt changes in vergence along length, a previously recognized characteristic of planetary and terrestrial thrust fault-related landforms (e.g. Plescia and Golombek, 1986; Byrne et al., 2014), are so commonly observed in this study that we do not record their locations. Often, multiple vergence changes are observed along a single landform (e.g. Fig. 8). These alternations in anticline asymmetry are observed along linear fault scarps and along bends where landform orientation changes dramatically. The region of vergence change shows three morphologies: (1) a smooth topographic high connecting two crests of anticlines associated with thrust fault-related landforms with opposite senses of asymmetry, (2) tips of adjacent thrust fault-related landforms wrapped concave inward towards each other, developing a small depression between the tips, or (3) greatly reduced topography in the region between the two landforms creating a featureless null space. Examples of each of these morphologies are shown in Fig. 8. A smooth transition between a south verging thrust fault-related landform and a northwest verging thrust fault following a crater rim illustrate the first type of transition (Fig. 8, example 1). In the central portion of the image, the western tip of a northward verging and the eastern tip of a southward verging thrust fault related landform arc toward each other, creating a <5 km wide depression (Fig. 8, example 2). To the south, an ~8 km long gap with very little topography separates northward verging and southward verging thrust fault-related landforms (Fig. 8, example 3).

Changes in vergence have been observed on thrust fault-related landforms on Mars (Watters, 1993) and within fold and thrust belts on Earth. In the Niger Delta Fold and Thrust Belt, changes in vergence are caused by antithetic fault interactions. Faults change vergence direction rapidly here due to their propagation from a weak basement décollement (Higgins et al., 2007; Davis and Engelder, 1985). In the Big Piney La Barge Field of the Cordilleran Thrust Belt antithetic faults also root to the same detachment surface resulting in anticlines with opposing senses of asymmetry (Greenhalgh et al., 2015). These studies conclude that the depth at which antithetic fault planes intersect determines the surface expression of the region between the oppositely verging anticlines. Faults that link only in the décollement produce none to small amounts of topography between their tips. If these faults propagate towards one another at shallow lithospheric depths, their tips may bend towards each other, forming small basins between the tips (Higgins et al., 2007). Some faults instead only intersect near the surface resulting in a fold connecting the two hanging wall anticlines and high topography (Higgins et al., 2007).

All three of the observed morphologies occur abundantly in the

Fig. 8. Examples of the morphologies associated with alternation in vergence direction along strike. MDIS mosaic overlain with MLA topography using orthographic projection centered at 80°N, 13°E. Example 1 shows a smooth transition between an anticline crest along a thrust fault-related landform and a crater rim bounded by a surface breaking thrust fault. Example 2 shows a small depression between the concave tips of multiple landforms. Example 3 shows a region between two oppositely verging landforms where no negative or positive topography has developed.

northern plains. In general, thrust fault-related landforms within the northern plains may exhibit an average overall orientation while many smaller segments along the thrust fault-related landform may deviate from that orientation. This results in small bends along the length of the thrust fault-related landform. Taken all observations together leads us to conclude that faults associated with these changes are likely rooted in a weak décollement below the northern plains. In most cases, our mapping suggests that folding precedes faulting. Individual conjugate faults may nucleate along the length of the folds and link up either in the décollement below the volcanic units or closer to the surface. As their surfaces intersect, the faults reshape the pre-existing fold producing clear changes in vergence direction, and sometimes strike, along the length of the thrust fault-related landform.

4. Discussion

4.1. Density of structures

We analyzed the density of thrust fault-related landforms within the northern plains (Fig. 9). Each landform with a unique identifying number was divided into ~1.5 km long segments. The coordinates of the centroid of each segment were calculated, and then the number of centroids per square kilometer was computed. Anticlines associated with mapped fault traces were filtered out of the calculation, as to not weight landforms with both anticlines and traces more heavily. This method of density calculation also prevented short and long faults from being weighted equally, as the numbers of segments, not faults themselves, were recorded.

The density of thrust-fault related landforms is greatly reduced near large superposing craters such as Rustaveli and Sousa (labeled with R and S in Fig. 9), which can be attributed to resurfacing and superposition of the associated ejecta blanket above thrust fault-related landforms. A higher density of landforms is also observed north of 70°N. Regions of greater landform density occur where few or small impact craters have been recorded, and thus, little resurfacing of those landforms has occurred. Because impact cratering reduces away from the ecliptic (Knibbe and van Westrenen, 2017), it is no surprise that the poles have fewer impacts.

We also compare the density of structures to the northern rise (Zuber et al., 2012). The northern rise is a dome-shaped uplift with a peak elevation of ~1.5 km and diameter of ~950 km estimated to postdate the northern plains emplacement (shown in Fig. 9). We do not observe any trends in density associated with the northern rise, which further supports that the uplift of the northern rise postdated the

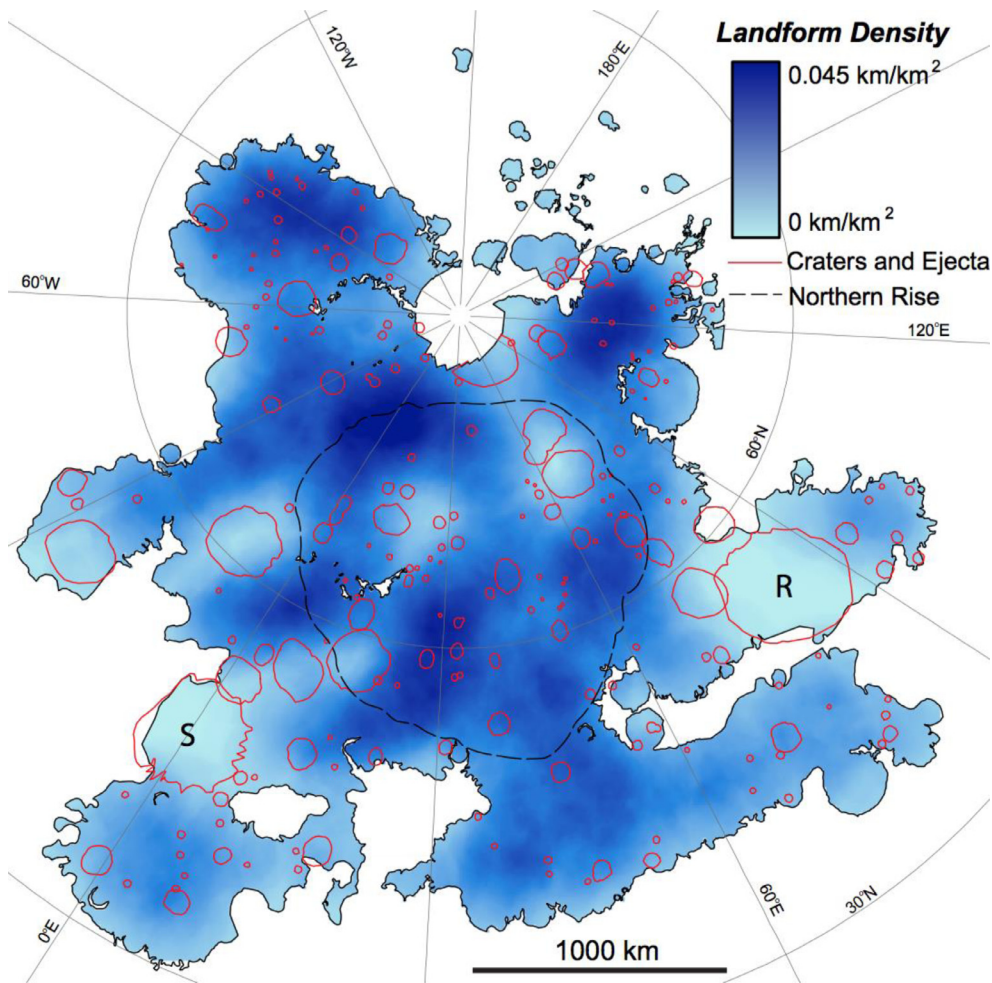


Fig. 9. Map of density of shortening landforms across the northern plains, with higher densities displayed in darker shades of blue. Landform density is expressed in kilometers of landform length per square kilometer (km/km^2). Craters and crater ejecta are outlined in red, the northern rise is outlined in a black dashed line, and the northern plains are outlined in solid black. Map is shown in stereographic projection centered at 30°E, 66°N. We observe denser regions of landforms to be found near the pole and in locations that lack large impact craters. We observe regions with fewer landforms to be those dominated by impacts. In particular, regions near relatively young craters host very few thrust fault-related landforms. Examples include Sousa (S) and Rustaveli (R) craters. Note that there is no obvious pattern in landform density associated with the northern rise. (For interpretation of the references to color in this figure legend, the reader is referred to the web version of this article.)

growth of the landforms in the northern plains (Dickson et al., 2012; Klimczak et al., 2012).

4.2. Orientation of structures

One aim of this study was to analyze the orientations of thrust fault-related landforms in the northern plains. This analysis was conducted by observing patterns recorded in representative rose diagrams across the plains. Again, fault traces and anticlines not associated with fault traces were divided into 1.5 km segments, and the azimuth of each was calculated. As with the density calculation, the separation of anticlines with and without fault traces and the division of landforms into segments was done to prevent weighting our calculations toward landforms with both anticlines and surface break traces or toward short landforms. We divided the northern plains into 20-degree by 20-degree bins. This bin size was chosen because it was large enough to (1) capture enough data points in each bin to feel confident in the calculated diagrams and (2) to prevent an effect of circularity from the largest impact craters. For example, if thrust fault-related landforms as part of a ghost crater were the only landforms in a bin, then the rose diagram would be expected to be nearly perfectly circular. However, if the bin size is much larger than the diameters of the large ghost craters, then orientations attributed to any regional or global pattern as opposed to pre-existing topography would be detectable. We wrote computer code using R to sort azimuths into bins of 20° and created rose diagrams color coded by our confidence in the represented landform orientations. Where more segments were recorded, we felt more confident in prescribing the orientations indicated by the rose diagrams, and where fewer segments were recorded, we felt less confident in the

orientations. We quantify our confidence only in the number of azimuths recorded (Fig. 10).

Rose diagrams generated from the orientations of fault segments showed a distinct bulls-eye pattern centered at the North Pole. From 90 to 70°N, faults are primarily oriented east-west. From 70 to 50°N, faults show no preferred orientation. In some bins in this latitude range, rose diagrams also appear to reflect mainly east-west landform orientations; however, these diagrams represent bins where only the northernmost portion of the bin contained northern plains units and associated thrust fault-related landforms. Therefore, the patterns in these rose diagrams more closely reflect orientation trends from the 90 to 70°N latitudinal band. Between 50 and 30°N, landforms are predominantly oriented north-south.

Although we recognize that a multitude of global and regional-scale processes, such as tidal despinning, subsidence, reorientation, and changes in orbital parameters may have the potential to influence orientations of thrust faults, especially when operating in concert with global contraction, fault patterns have historically been discussed with a focus on tidal despinning. Many studies predict latitude dependent landform orientations if stresses related to tidal despinning contributed to the growth of the tectonic fabric (e.g. Pechmann and Melosh, 1979; Dombard and Hauck, 2008; Beuthe, 2010; Klimczak et al., 2015). In particular, tidal despinning was proposed to result in east-west normal faulting near the poles and north-south thrust faulting near the equator (e.g., Pechmann and Melosh, 1979). The interpretations from these models assumed that Anderson's Theory of Faulting was applicable to tensile stresses near the poles; however, tensile stresses produce jointing, not faulting (Klimczak et al., 2015). Furthermore, Klimczak et al. (2015) show that normal faulting is not induced at

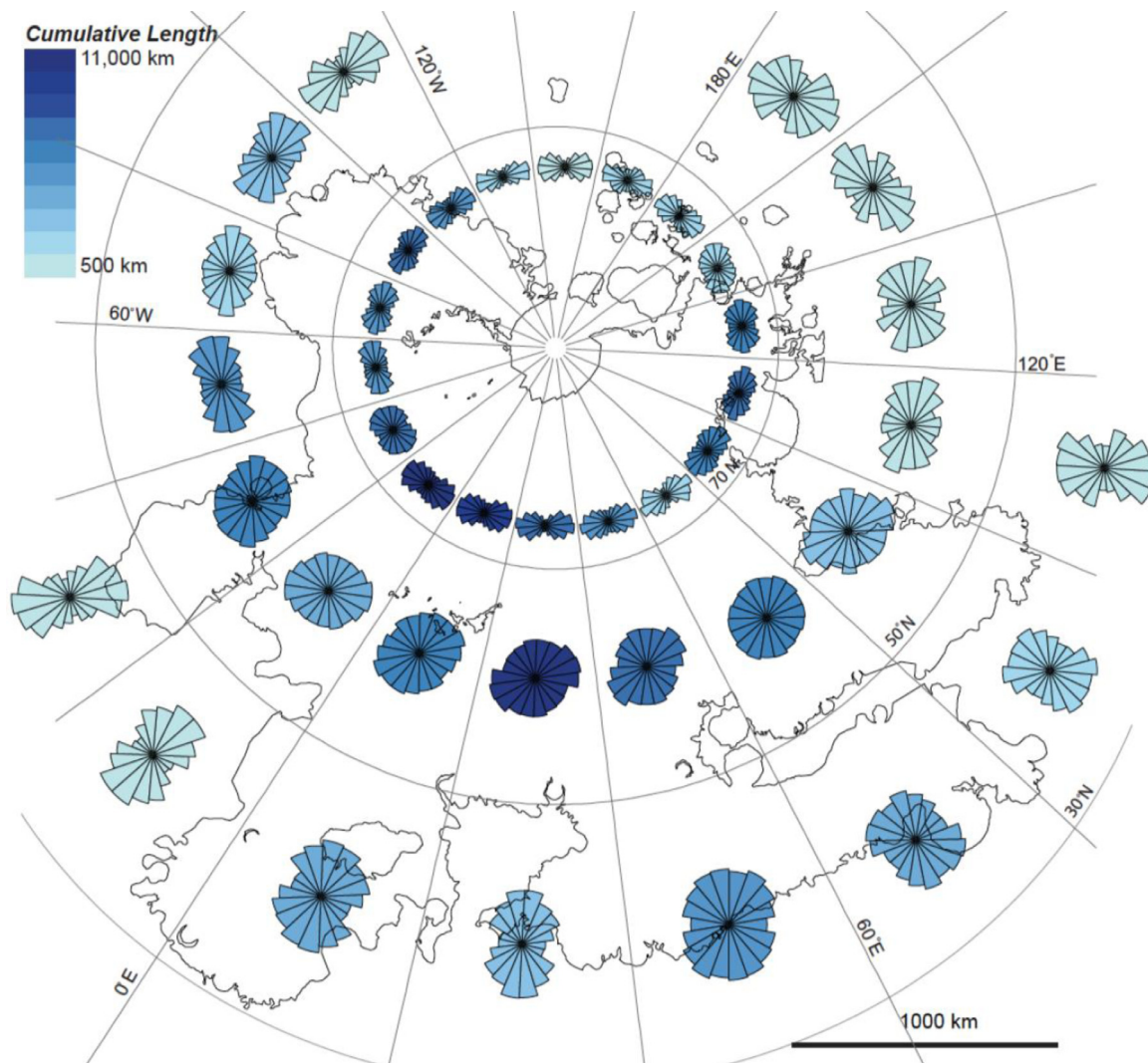


Fig. 10. Orientations of thrust fault-related landforms across the northern plains. Rose diagrams representing fault orientations within 20° latitude by 20° longitude bins are shown in blue and are oriented poleward. Deeper blues indicate more fault segments from which azimuths could be calculated, and therefore convey more confidence in the diagram. The map is shown in stereographic projection centered at 30°E, 66°N. Note the preferential orientations of thrust fault-related landforms and the change of preferred orientation with latitude. (For interpretation of the references to color in this figure legend, the reader is referred to the web version of this article.)

depths greater than ~20 km near 60° latitude as a consequence of increasing overburden stresses.

If all stresses were compressive (as is implied in Anderson's Theory of Faulting), to produce east-west oriented normal faults near the poles, stresses would have to be large enough to overcome the frictional resistance to sliding and thus can be assessed with the Coulomb Criterion. We find that magma or some other fluid would have been necessary in fractures to induce failure. If the east-west oriented thrust faults associated with landforms observed near the poles are not a product of reactivated normal faults but instead initially formed due to thrust faulting, then the presence of fluid in fractures, uplift, the removal of overburden possibly from a large impact, or added stress from global contraction would have been a prerequisite to rock failure.

Subsidence concentrates maximum horizontal compressive stresses within depressed regions such as those filled with volcanic deposits. This process is expected to result in an increased frequency of thrust fault related-landforms within volcanically flooded impact basins and specific to Mercury, within the northern plains as a whole (Watters et al., 2009; Freed et al., 2012). The Caloris impact, which modified a substantial area of Mercury, is thought to have taken place before the emplacement of the smooth plains (Fassett et al., 2009). Models of the

reorientation of Mercury's pole of rotation due to the loading of the Caloris basin, when combined with the effects of tidal despinning and global contraction, predict maximum principle stresses to be compressive and horizontal, but with varied orientations (Matsuyama and Nimmo, 2009). The orientations of these stresses are determined by the degree of tidal despinning and reorientation. These models predict a tectonic pattern consisting of radially oriented thrust faults about the initial pole of rotation and north-south oriented thrust faults within the initial equatorial region. Because the initial pole must now be south of the current pole, originally radial and north-south oriented faults would now appear slightly east-west oriented (Matsuyama and Nimmo, 2009). Additionally, some changes in orbital parameters, such as those that induce changes in tides on the Moon (Watters et al., 2015b), may have caused similar changes in solar tides for Mercury. These stresses while not great enough to cause faulting, may have contributed to changes in fault orientation. Since patterns caused by these sources have not yet been predicted for Mercury, we cannot compare them to our observations.

As has been previously suggested for Mercury (e.g. Dzurisin, 1978; Dombard and Hauck, 2008; Matsuyama and Nimmo, 2009; Klimczak et al., 2015) and for the Moon (e.g. Watters et al., 2015b) some

combination of the aforementioned processes likely acted in concert to influence the type and orientations of tectonic landforms to varying degrees. The timing of these processes is critical to establishing the geologic history of Mercury, and that timing can be discerned by comparing observations of tectonic patterns with those predicted to result from stresses associated with those geologic processes, either individually or in concert. Because the northern plains have been dated to $\sim 3.7\text{--}3.9$ Ga (Denevi et al., 2013; Ostrach et al., 2015), opening mode fractures must have been present in the lithosphere around this time in order to facilitate the movement of large amounts of volcanic materials to the surface. It is possible that pre-existing favorably oriented discontinuities were reactivated after the formation of the northern plains, and so patterns and orientations within the plains may be basement-controlled and thus reflective of earlier processes.

We propose two possible geologic histories for Mercury that may explain our observations: one in which reorientation due to the Caloris impact occurs and one in which it does not. Because the pattern of thrust fault-related landform orientations is circumpolar, the first scenario requires any major reorientation of the planet due to the Caloris impact to have predated the formation of thrust fault-related landforms in the northern plains and if their orientations are linked to tidal despinning (or any other process that influenced their pattern) then it must have also predated those processes. After reorientation, tidal despinning and/or these other processes established a tectonic fabric of east–west oriented lithospheric weaknesses. As impacts shaped the heavily cratered terrain, a regolith layer developed across Mercury. The opening mode fractures and normal faults associated with reorientation, tidal despinning, and/or other processes may have facilitated effusive volcanism that formed the smooth plains. A lack of smooth plains in the southern hemisphere (Denevi et al., 2013) could indicate that reorientation due to the Caloris impact caused preferential faulting and therefore opening of magma pathways in the northern hemisphere. These discontinuities also contributed to the orientations of thrust fault-related landforms that would later characterize the northern plains, either via reactivation of normal faults or as basement-influenced deformation. The deformation style of these particular landforms is discussed in more detail in Section 4.3.

In the second scenario, in which reorientation due to the Caloris impact did not occur, tidal despinning or any other processes influencing fault patterns cannot be temporally tied to the Caloris impact. But even in this scenario, fault reactivation and basement-controlled deformation along structures established by global contraction and tectonic processes predating plains emplacement could have influenced fault orientations within the northern plains. If however, orientations or faults within the smooth plains were not influenced by pre-existing basement faults, then the processes responsible for the observed tectonic pattern must have been active after plains emplacement.

Previous authors have also found through analysis of thrust fault-related landform orientations that tidal despinning likely played a role in the development of Mercury's global tectonic fabric (e.g., Watters et al., 2015a). Other studies have suggested that the tectonic patterns, including orientation and density of landforms, observed could have resulted from despinning along with mantle downwelling, pole reorientation, and/or changes in lithospheric thickness (e.g. King, 2008; Matsuyama and Nimmo, 2009; Beuthe, 2010). Beuthe (2010) produces a model for thrust fault orientation distribution with a mid-latitude transition between north-south oriented thrust faults and east-west oriented thrust faults, similar to the mapping results of this work. King (2008) suggests that mantle downwelling concentrates the locations of lobate scarps, a conclusion supported by Watters et al. (2015a). We do not find any evidence to support this conclusion in the density of thrust fault-related landforms in the northern plains. Aside from evidence of faulting removed by impact cratering processes, we do not observe any pattern in fault density.

4.3. Thin-skinned vs. thick-skinned deformation in the northern plains

One goal of this study was to determine the subsurface fault architecture and tectonic style associated with deformation in the northern plains. We aimed to determine if shortening was confined to the plains units or if it extended into the basement. On Earth, if surficial units are mechanically decoupled from units below due a weak layer, deformation is accommodated in the upper units, and the style of tectonism is referred to as “thin-skinned” deformation (Chapple, 1978). The northern plains may be underlain by a weak, regolith layer developed through impact processes (Marchi et al., 2013) that was later buried by volcanism. On the contrary, if faulting roots deep into the basement, the style of tectonism is called “thick-skinned” deformation (Coward, 1983). A third style implies a structural link between the basement and upper units where faults within the basement may contribute to orientation and development of faults in the upper units, and this style of tectonism is called “basement-involved thin-skinned” deformation (Pfiffner, 2017). Basement-involved thin-skinned tectonism occurs in locations such as the Central Apennines of Italy, the Jura fold and thrust belt in France, and the northwestern portion of the Taiwan fold and thrust belt (Tozer et al., 2002; Lacombe et al., 2003; Madritsch et al., 2008). In these mountain belts, faults in shallow layers develop above, but are linked to older (pre-existing) faults in the basement while overall displaying tectonic styles associated with thin-skinned deformation.

We observe compound landforms that by analogy with landforms seen on Earth and other planets and/or models, primarily reflect thin-skinned tectonics (see Section 3). A weak layer of regolith formed before effusive volcanism took place may have produced the décollement necessary to partition strain into the plains units only. Detachment thrust faults could propagate upward from this décollement or from the interface between volcanic units and impact crater walls and floors. Faults following crater rims, broad linear to arcuate rises of equal width, parallel evenly spaced ridges, and changes in vergence all imply the presence of faults that root to shallow décollements. Sigmoidal rises may be related to linkage of low angle thrust faults, but require steeply dipping but not necessarily deep faults for connectivity. V-shaped rises may reflect faults that root to the base of thin or thick upper units, and require fault interactions at some depth.

Aside from our analysis of analogues and models, our fault orientation analysis indicates that thrust-fault related landforms could have inherited their orientations from buried, pre-existing faults and other weaknesses that formed prior to emplacement of the northern plains but were reactivated at a later time. Sigmoidal rises interpreted to be step-overs and restraining bends likely develop their orientations from the process of transfer of slip between faults, and faults propagating along crater walls are proposed to draw their orientations and curvature from the interface of the crater wall and overlying volcanic unit itself. However, as described above, V-shaped rises, broad rises, proposed fold and thrust belts, and landforms with changes in vergence are all indicative of landforms underlain by faults rooting to shallow décollements. The regolith-related contact between the cratered terrain basement and volcanic flood units could function as one such décollement horizon. If the orientations of thrust faults beneath these landforms reflect possible geologic processes that deformed the basement rocks and could have allowed for the emplacement of effusive volcanic deposits, then it is possible that thrust fault orientations and locations are inherited, or controlled, by basement faults. Deformation in the northern plains could therefore be more accurately represented with basement-involved thin-skinned tectonics instead of thin-skinned tectonics alone. If deformation is not related to basement faults, then the geologic processes resulting in the observed tectonic pattern must have occurred after the emplacement of the volcanic units. The degree of involvement of basement faults should be tested in the future by fitting finite-element models or forward fault-geometry models to topography.

In short, we observe a tectonically complex planet with local and regional landform patterns indicative of varied subsurface structure. While many faults may shallowly root to a weak layer, others may penetrate deeper into the subsurface, linking with ancient basement structures. Like the analogues for the aforementioned compound landforms, this complexity reflects some of the breadth of deformation styles observed on Earth.

5. Conclusions

We produced a detailed map of anticlines and fault scarps within the northern plains in order to describe common shortening-related landform morphologies in the region with the aim to distinguish between thin- and thick-skin deformation styles. In addition, the orientations of landforms across the northern plains helped us to establish the relative timing of northern plains emplacement with respect to processes that may have led to the observed landform orientation, such as tidal despinning and pole reorientation.

Thrust fault-related landforms of the northern plains were mapped using MESSENGER datasets in unprecedented detail. Combining our structural interpretation of map patterns and imagery allowed for the interpretation of landform geology. The landforms we observe represent the broad spectrum of tectonic morphologies. Thrust fault-related landforms do occur in isolation, but we find that they often transition into one another or exist in map patterns that imply that they are structurally connected below the surface.

Five compound landforms and one common structural characteristic were identified, all of which support a model of thin-skinned or basement-involved thin-skinned deformation within the northern plains volcanic unit. As faults grew, they likely rooted into a regolith décollement producing pop up structures of approximately equal width and anticlines with opposing vergence. Locally, thin regolith may have allowed for a stronger décollement. The presence of this décollement combined with an early rapid pulse of global contraction, could have produced the development of relatively narrow fold and thrust belts. Flooded and buried impact craters and basins may have localized stresses along their walls and rims, contributing to the development of wrinkle-ridge-rings. These same craters, basins, and also other areas, especially those coinciding with gravity lows redirected fault surfaces producing V-shaped rises. As some faults propagated towards each other, sigmoidal rises interpreted as step-overs linked the faults and accommodated oblique slip.

Based on the pattern of preferred orientations of thrust fault-related landforms across the northern plains (Fig. 10), some other geological process(es) besides global contraction, such as tidal despinning, influenced the orientations of faults underlying these landforms, contributing to latitudinal patterns in fault orientation. The pattern indicates a circum-polar orientation of thrust fault-related landforms, which establishes that no planetary reorientation occurred after the formation of these landforms. If tidal despinning governed the preferred orientations of these landforms, it may have occurred very early, deforming the lithosphere to produce opening mode fractures and normal faults, and allowing for the emplacement of the northern plains. These weaknesses would then later have been reactivated as discontinuities in the basement by global contraction, where they influenced the orientation and location of thrust fault-related landforms forming in the overlying volcanic plains.

Acknowledgments

CK was funded by the Discovery Data Analysis Program under grant NNX16AK23G. We thank the handling editor, Francis Nimmo, as well as Valentina Galluzzi and an anonymous reviewer for their helpful comments on this research.

References

- Allemand, P., Thomas, P.G., 1995. Localization of Martian ridges by impact craters: mechanical and chronological implications. *J. Geophys. Res.* 100, 3251–3262.
- Anderson, E.M., 1951. The Dynamics of Faulting and Dyke Formation with Applications to Britain. Oliver and Boyd, Edinburgh.
- Banks, M.E., et al., 2015. Duration of activity on lobate-scarp thrust faults on Mercury. *J. Geophys. Res.* 120, 1751–1762.
- Beuthe, M., 2010. East-west faults due to planetary contraction. *Icarus* 209, 795–817.
- Bilotti, F., Suppe, J., 1999. The global distribution of wrinkle ridges on Venus. *Icarus* 139, 137–157.
- Blakely, R.J., Sherrod, B.L., Weaver, C.S., Wells, R.E., Rohay, A.C., 2014. The Wallula fault and tectonic framework of south-central Washington, as interpreted from magnetic and gravity anomalies. *Tectonophysics* 624–625, 32–45.
- Byrne, P.K., et al., 2015. Deep-seated thrust faults bound the Mare Crisium lunar mascon. *Earth Planet. Sci. Lett.* 427, 183–190.
- Byrne, P.K., Klimczak, C., Celal Sengor, A.M., Solomon, S.C., Watters, T.R., Hauck, S.A., 2014. Mercury's global contraction much greater than earlier estimates. *Nat. Geosci.* 7, 301–307.
- Casale, G., Pratt, T.L., 2015. Thin- or thick-skinned faulting in the Yakima Fold and Thrust Belt (WA)? Constraints from the kinematic modeling of the Saddle Mountains anticline. *Bull. Seismol. Soc. Am.* 105, 745–752.
- Chapple, W.M., 1978. Mechanics of thin-skinned fold-and-thrust belts. *Geol. Soc. Am. Bull.* 89, 1189–1198.
- Couzens-Schultz, B.A., Vendeville, B.C., Wiltschko, D.V., 2003. Duplex style and triangle zone formation insights from physical modeling. *J. Struct. Geol.* 25, 1623–1644.
- Coward, M.P., 1983. Thrust tectonics, thin skinned or thick skinned, and the continuation of thrusts to deep in the crust. *J. Struct. Geol.* 5, 113–123.
- Cowie, P.A., Scholz, C.H., 1992. Physical explanation for the displacement-length relationship of faults using a post-yield fracture mechanics model. *J. Struct. Geol.* 14, 1133–1148.
- Crane, K.T., Klimczak, C., 2017. Timing and rate of global contraction on Mercury. *Geophys. Res. Lett.* 44, 3082–3089.
- Davis, D.M., Engelder, T., 1985. The role of salt in fold-and-thrust belts. *Tectonophysics* 119, 67–88.
- Denevi, B.W., et al., 2013. The distribution and origin of smooth plains on Mercury. *J. Geophys. Res.* 118, 891–907.
- Dickson, J.L., et al., 2012. Topographic rise in the northern smooth plains: characteristics from MESSENGER image and altimetry data and candidate modes of origin. *Lunar Planet. Sci. XLIII*, 2239 (abstract).
- Dombard, A.J., Hauck, S.A., 2008. Despinning plus global contraction and the orientation of lobate scarps on Mercury: prediction for MESSENGER. *Icarus* 198, 274–276.
- Dzurisin, D., 1978. The tectonic and volcanic history of Mercury as inferred from studies of scarps, ridges, troughs, and other lineaments. *J. Geophys. Res.* 83, 4883–4906.
- Fassett, C.I., et al., 2012. Large impact basins on Mercury: global distribution, characteristics, and modification history from MESSENGER orbital data. *J. Geophys. Res.* 117.
- Fassett, C.I., et al., 2009. Caloris impact basin: exterior geomorphology, stratigraphy, morphometry, radial sculpture, and smooth plains deposits. *Earth Planet. Sci. Lett.* 285, 297–308.
- Freed, A.M., et al., 2012. On the origin of graben and ridges within and near volcanically buried craters and basins in Mercury's northern plains. *J. Geophys. Res.* 117, E00L06.
- Golombek, M.P., Anderson, F.S., Zuber, M.T., 2001. Martian wrinkle ridge topography: evidence for subsurface faults from MOLA. *J. Geophys. Res.* 106, 23811–23821.
- Golombek, M.P., Plescia, J.B., Franklin, B.J., 1991. Faulting and folding in the formation of wrinkle ridges. *Proc. Lunar Sci. Conf.* 21, 679–693.
- Greenhalgh, S.R., McBride, J.H., Bartley, J.M., Keach, R.W., Britt, B.B., Kowallis, B.J., 2015. Along-strike variability of thrust fault vergence. *Interpretation* 3, SX1–SX12.
- Head, J.W., et al., 2011. Flood volcanism in the northern high latitudes of Mercury revealed by MESSENGER. *Science* 333, 1853–1855.
- Higgins, S., Davies, R.J., Clarke, B., 2007. Antithetic fault linkages in a deep water fold and thrust belt. *J. Struct. Geol.* 29, 1900–1914.
- Jadoon, I.A.K., Lawrence, R.D., Hassan, K.S., 1994. Mari-Bugdi pop-up zone in the central Sulaiman fold belt, Pakistan. *J. Struct. Geol.* 16, 147–158.
- Jaeger, J.C., Cook, N.G.W., Zimmerman, R.W., 2007. Fundamentals of Rock Mechanics, 4th ed. Blackwell Publishing, Malden, MA.
- Kinczyk, M.J., Prockter, L.M., Chapman, C.R., Susorney, H.C.M., 2016. A morphological evaluation of crater degradation on Mercury: revisiting crater classification using MESSENGER data. *Lunar Planet. Sci. Conf. XLVII*, 1537 (abstract).
- King, S.D., 2008. Pattern of lobate scarps on Mercury's surface reproduced by a model of mantle convection. *Nat. Geosci.* 1, 229.
- Klimczak, C., et al., 2012. Deformation associated with ghost craters and basins in volcanic smooth plains on Mercury: strain analysis and implications for plains evolution. *J. Geophys. Res.* 117.
- Klimczak, C., Byrne, P.K., Solomon, S.C., 2015. A rock mechanical assessment of Mercury's global tectonic fabric. *Earth Planet. Sci. Lett.* 416, 82–90.
- Knibbe, J.S., van Westrenen, W., 2017. On Mercury's past rotation, in light of its large craters. *Icarus* 281, 1–18.
- Lacombe, O., Moutheau, F., Angelier, J., Chu, H., Lee, J., 2003. Frontal belt curvature and oblique ramp development at an obliquely collided irregular margin: geometry and kinematics of the NW Taiwan fold-thrust belt. *Tectonics* 22.
- Long, S., McQuarrie, N., Tobgay, T., Grujic, D., 2010. Geometry and crustal shortening of the Himalayan fold-thrust belt, eastern and central Bhutan. *Geol. Soc. Am. Bull.* 1–21.
- Madritsch, H., Schmid, S.M., Fabbri, O., 2008. Interactions between thin- and thick-skinned tectonics at the northwestern front of the Jura fold-and-thrust belt (eastern

- France). *Tectonics* 27.
- Mangold, N., Allemand, P., Thomas, P.G., 1998. Wrinkle ridges of Mars: structural analysis and evidence for shallow deformation controlled by ice-rich décollements. *Planet. Space Sci.* 46, 345–356.
- Mann, P., 2007. Global Catalogue, Classification and Tectonic Origins of Restraining- and Releasing Bends On Active and Ancient Strike-Slip Fault Systems. *Geol. Soc. Lond. Spec. Publ.* 290, 13–142.
- Marchi, S., Chapman, C.R., Fassett, C.I., Head, J.W., Bottke, W.F., Strom, R.G., 2013. Global resurfacing of Mercury 4.0–4.1 billion years ago by heavy bombardment and volcanism. *Nature* 499, 59–61.
- Massironi, M., 2015. Lateral ramps and strike-slip kinematics on Mercury. *Geol. Soc. Lond. Spec. Publ.* 401, 269–290.
- Matsuyama, I., Nimmo, F., 2009. Gravity and tectonic patterns of Mercury: effect of tidal deformation, spin-orbit resonance, nonzero eccentricity, despinning, and reorientation. *J. Geophys. Res.* 114, E1.
- Mazarico, E., et al., 2014. The gravity field, orientation, and ephemeris of Mercury from MESSENGER observations after three years in orbit. *J. Geophys. Res.* 119, 2417–2436.
- McClay, K., Bonora, M., 2001. Analog models of restraining stepovers in strike-slip fault systems. *AAPG Bull.* 85, 233–260.
- Melosh, H.J., 1989. Impact Cratering: A Geologic Process. *Impact Cratering: A Geologic Process*. Oxford University Press, New York.
- Melosh, H.J., Dzurisin, D., 1978. Mercurian global tectonics: a consequence of tidal despinning? *Icarus* 35, 227–236.
- Melosh, H.J., 1977. Global tectonics of a despun planet. *Icarus* 31, 221–243.
- Mitra, S., Paul, D., 2011. Structural geometry and evolution of releasing and restraining bends: insights from laser-scanned experimental models. *Am. Assoc. Petrol. Geol. Bull.* 95, 1147–1180.
- Montési, L.G.J., Zuber, M.T., 2003. Spacing of faults at the scale of the lithosphere and localization instability: 2. Application to the Central Indian Basin. *J. Geophys. Res.* 108.
- Neel, C.R., Mueller, K., 2007. Structural analysis of wrinkle-ridge rings on Lunae and Hesperia Planum, Mars: evidence of buried topography. *Lunar Planet. Sci. XXXVIII*, 2185 (abstract).
- Ostrach, L.R., et al., 2015. Extent, age, and resurfacing history of the northern smooth plains on Mercury from MESSENGER observations. *Icarus* 250, 602–622.
- Paylor, E.D., Yin, A., 1993. Left-slip evolution of the North Owl Creek fault system, Wyoming during Laramide Shortening. *Geol. Soc. Am. Spec. Pap.* 280, 229–242.
- Pechmann, J.B., Melosh, H.J., 1979. Global fracture patterns of a despun planet: application to Mercury. *Icarus* 38, 243–250.
- Peterson, G.A., Johnson, C.L., Byrne, P.K., Phillips, R.J., Neumann, G.A., 2017. Depth of faulting in Mercury's northern hemisphere from thrust fault morphology. *Lunar Planet. Sci. XLVIII*, 2315 (abstract).
- Pfiffner, O.A., 2017. Thick-skinned and thin-skinned tectonics: a global perspective. *Geosciences* 7.
- Plescia, J.B., Golombek, M.P., 1986. Origin of planetary wrinkle ridges based on the student of terrestrial analogs. *Geol. Soc. Am. Bull.* 97, 1289–1299.
- Schultz, R.A., 2000. Localization of bedding plane slip and backthrust faults above blind thrust faults: keys to wrinkle ridge structure. *J. Geophys. Res.* 105, 12035–12052.
- Solomon, S.C., 1978. On volcanism and thermal tectonics on one-plate planets. *Geophys. Res. Lett.* 5, 461–464.
- Solomon, S.C., 1976. Some aspects of core formation in Mercury. *Icarus* 28, 509–521.
- Spudis, P.D., Guest, J.E., 1988. Stratigraphy and geologic history of Mercury. In: Vilas, F., Chapman, C.R., Matthews, M.S. (Eds.), *Mercury*. University of Arizona Press, Tucson, Ariz, pp. 118–164.
- Strom, R.G., et al., 2011. Mercury crater statistics from MESSENGER flybys: implications for stratigraphy and resurfacing history. *Planet. Space Sci.* 59, 1960–1967.
- Strom, R.G., Trask, N.J., Guest, J.E., 1975. Tectonism and volcanism on Mercury. *J. Geophys. Res.* 80, 2478–2507.
- Susorney, H.C.M., Barnouin, O.S., Ernst, C.M., Byrne, P.K., 2017. The surface roughness of Mercury from the Mercury Laser Altimeter: investigating the effects of volcanism, tectonism, and impact cratering. *J. Geophys. Res.* 122, 1372–1390.
- Tozer, R.S.J., Butler, R.W.H., Corrado, S., 2002. Comparing Thin- and Thick-Skinned Thrust Tectonic Models of the Central Apennines, Italy. *EGU Stephan Mueller Special Publication Series* 1, pp. 181–194.
- Vermilye, J.M., Scholz, C.H., 1998. The process zone: a microstructural view of fault growth. *J. Geophys. Res.* 103, 12223–12237.
- Walsh, L.S., Watters, T.R., Banks, M.E., Solomon, S.C., 2013. Wrinkle ridges on Mercury and the Moon: a morphometric comparison of length–relief relations with implications for tectonic evolution. *Lunar Planet. Sci. XLIV*, 2937 (abstract).
- Watters, T.R., Selvans, M.M., Banks, M.E., Hauck, S.A., Becker, K.J., Robinson, M.S., 2015a. Distribution of large-scale contractional tectonic landforms on Mercury: implications for the origin of global stresses. *Geophys. Res. Lett.* 42, 3755–3763.
- Watters, T.R., et al., 2015b. Global thrust faulting on the Moon and the influence of tidal stresses. *Geology* 43, 851–854.
- Watters, T.R., et al., 2012. Extension and contraction within volcanically buried impact craters and basins on Mercury. *Geology* 40, 1123–1126.
- Watters, T.R., et al., 2009. The tectonics of Mercury: the view after MESSENGER's first flyby. *Earth Planet. Sci. Lett.* 285, 283–296.
- Watters, T.R., 2004. Elastic dislocation modeling of wrinkle ridges on Mars. *Icarus* 171, 284–294.
- Watters, T.R., Robinson, M.S., Bina, C.R., Spudis, P.D., 2004. Thrust faults and the global contraction of Mercury. *Geophys. Res. Lett.* 31.
- Watters, T.R., Cook, A.C., Robinson, M.S., 2001. Large-scale lobate scarps in the southern hemisphere of Mercury. *Planet. Space Sci.* 49, 1523–1530.
- Watters, T.R., Robinson, M.S., 1999. Lobate Scarps and the martian crustal dichotomy. *J. Geophys. Res.* 104, 18981–18990.
- Watters, T.R., 1993. Compressional tectonism on Mars. *J. Geophys. Res.* 98, 17049–17060.
- Watters, T.R., 1989. Periodically spaced anticlines of the Columbia Plateau. In: Reidel, S.P., Hooper, P.R. (Eds.), *Volcanism and Tectonism in the Columbia River Flood-Basalt Province*. 239. *Geol. Soc. Am. Special Papers*, pp. 283–292.
- Watters, T.R., 1988. Wrinkle ridge assemblages on the terrestrial planets. *J. Geophys. Res.* 93, 10236–10254.
- Wood, C.A., et al., 2005. The Lamont-Gardner megadome alignment: a lunar volcanotectonic structure? *Lunar Planet. Sci. XXXVI*, 1116 (abstract).
- Wright, J., Rothery, D.A., Balme, M.R., Conway, S.J., 2018. Geological Mapping of the Hokusaï (H05) quadrangle of Mercury: status update. *Lunar Planet. Sci. XLIX*, 2164 (abstract).
- Young, W.C., Budynas, R.G., 2002. Stress concentration factors. *Roark's Formulas for Stress and Strain*. McGraw-Hill, New York, pp. 771–799.
- Yue, Z., Li, W., Di, K., Liu, Z., Liu, J., 2015. Global mapping and analysis of lunar wrinkle ridges. *J. Geophys. Res.* 120, 978–994.
- Zuber, M., et al., 2012. Topography of the Northern Hemisphere of Mercury from MESSENGER laser altimetry. *Science* 336, 217–219.